

Entanglement transfer via Chiral Quantum Walk on a Triangular Chain

Utku Sağlam,^{1,*} Mauro Paternostro,^{2,†} and Özgür E. Müstecaplıoğlu^{3,4,‡}

¹*Department of Physics, 1150 University Avenue, University of Wisconsin at Madison, Madison, Wisconsin 53706, USA*

²*Centre for Theoretical Atomic, Molecular, and Optical Physics,*

School of Mathematics and Physics, Queen's University, Belfast BT7 1NN, United Kingdom

³*Department of Physics, Koç University, Sarıyer, İstanbul, 34450, Turkey*

⁴*TÜBİTAK Research Institute for Fundamental Sciences, 41470 Gebze, Turkey*

(Dated: December 23, 2024)

We investigate the chiral quantum walk (CQW) for entanglement transfer on a triangular chain. We specifically consider two site Bell-type entangled cases. Using concurrence as quantum entanglement measure, together with the Bures distance as the measure of the fidelity of the state transfer, we evaluate the success of the entanglement transfer. We compare the entangled state transfer time and quality in CQW against a continuous-time quantum random walk.

I. INTRODUCTION

Fast and accurate one-way transmission of quantum states through communication or computation networks is a critical objective for quantum technologies [1–3]. Proposed schemes to achieve this goal consider engineered couplings between the network sites [4–13], external fields [14–17], weak measurements [18, 19], or transport in noisy environments of biological or synthetic systems [20–24]. Such methods are challenging to implement in practice for profound quantum states, such as quantum entanglement transfer, due to quantum decoherence and disorder [25, 26].

Pretty-good State Transfer (PGST) can be achieved on dual-spin chains [27], spin chains with weakly coupled endpoints [7, 28–31] and projective measurements [32] with Quantum Walk (QW) schemes. Continuous time quantum walk (CTQW) is a paradigmatic model of quantum transport [33, 34]. Both discrete [35, 36] and continuous [37–40] time quantum walks have been discussed for pretty good state transfer. CTQW can be made one way by taking complex-valued couplings, which is called a chiral quantum walk (CQW) [41–43]. Chirality emerges due to the breaking of time-reversal symmetry (TRS) [44], and it provides a significant boost to the transport speed [41].

The existence of high-dimensional entanglement is advantageous in quantum communication [45] and quantum superdense coding [46–48]. The perfect transfer of states in spin chains paves the way for the creation of required entangled states and logic gate structures for quantum computation and quantum information [49, 50]. These multi-dimensional entangled states can be produced by repeatedly generating the entanglement in a low-dimensional system and transferring these to a higher dimensional one [51]. Our goal is to explore if CQW can be used to transmit two and three-dimensional quantum entangled states; what are the possible advantages it may offer regarding distance, speed, and transfer quality?

We specifically consider CQW on a linear chain of equilateral triangles, as shown in Fig. 1, which is the simplest

graph that allows for so-called probability time symmetry (PTS) breaking [42]. A walker can transfer from one node to any other neighboring site on the triangular plaquette by passing through either one or two edges. We consider a uniform complex coupling between the nearest-neighbor sites. Due to the path length difference between odd and even number of edges traveled, and phases of the complex couplings, interference can enhance the transfer rate. For a triangular plaquette, the maximum asymmetry in forward and backward time evolution is found when the phase of the couplings is $\theta = \pi/2$ [42].

The spatial entanglement in the site basis can be defined in quantum walks [52, 53]. The system's initial state is taken to be a qubit in a spatially entangled state. Consequently, this spatially entangled qubit state is injected into the chain from the left. We consider two-site spatial entanglement to explore the chiral transfer of Spatially Bell Entangled States, which are significant for quantum communication and computation [54]. The quality of the transfer is examined by calculating the density matrix, concurrence [55], fidelity, and Bures distances explicitly [56–58]. Besides, we compared the time of transfer to characterize the speed-up advantage of CQW. In addition, we numerically confirm that the entanglement state transfer speed indeed linearly scales with the chain size [74–76].

The triangular chain lattice can be realized in superconducting circuits [59, 60], trapped ions [61], NMR systems [42], photonic and spin waveguides [62], and in optical lattices [63]. In the case of optical lattices, complex edge weights could be introduced with the help of artificial gauge fields [64, 65], nitrogen vacancy centers in diamonds [66] or with plasmonic non-Hermitian coupled waveguides [67].

This paper is organized as follows. We introduce the CQW on a triangular chain model by presenting the adjacency matrix and present the associated Hamiltonian model with complex hopping rates in Sec. II. Our results are given in Sec. III in five subsections. PTS breaking and entanglement transfer in CTQW and CQW on a triangular chain are discussed in Sec. III A and Sec. III B, respectively.

* Electronic address: usaglam@wisc.edu

† Electronic address: m.paternostro@qub.ac.uk

‡ Electronic address: omustecap@ku.edu.tr

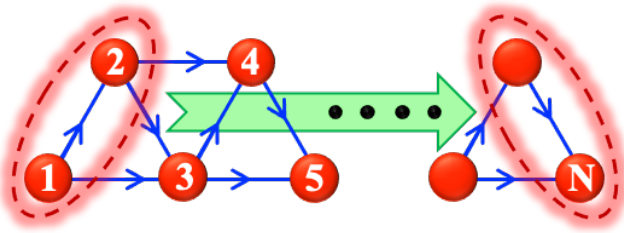


Figure 1. Graph of a linear chain of N vertices arranged in triangular plaquettes. Initially, the pair of sites 1 and 2 at the left end of the chain are entangled. The entangled state is transported to the rightmost pair of vertices ($N-1$ and N) after a chiral quantum walk. Arrows indicate the directed edges with complex weight factors, taken to be $+i$. In the opposite direction, the weight factors change phase and become $-i$. We have also examined transferring three-site entanglement from the leftmost plaquette (1, 2 and 3) to the right end of the chain.

II. MODEL SYSTEM: CQW ON A TRIANGULAR CHAIN

We consider CQW on a triangular chain of N vertices as shown in Fig. 1. Triangular chain is a minimal graph where PTS can be broken [42] so that $P_{nm}(t) \neq P_{mn}(t)$ or $P_{nm}(t) \neq P_{nm}(-t)$, where $P_{nm}(t)$ ($P_{nm}(-t)$) is the transition probability between the nodes n and m going forward (backward) in time. Breaking of PTS allows for enhanced quantum transport by CQW [41, 43].

We will use the site basis $\{|i\rangle\}$, with $i = 1..N$ indicating which site is occupied such that $|i\rangle := |0_1, 0_2, \dots, i_1, \dots, 0_N\rangle$. The set of coupled sites in a graph determine the edges $e = (i, j)$, which can be described by the so-called adjacency matrix A [68–71]. For a triangular chain of $N = 5$ sites, A is given by

$$A = \begin{bmatrix} 0 & 1 & 1 & 0 & 0 \\ 1 & 0 & 1 & 1 & 0 \\ 1 & 1 & 0 & 1 & 1 \\ 0 & 1 & 1 & 0 & 1 \\ 0 & 0 & 1 & 1 & 0 \end{bmatrix}. \quad (1)$$

Together with the degree matrix D for the self edges (i,i), A , determines the graph Laplacian $L = D - A$. Hamiltonian of the walk is given by the Hadamard product $H = J \circ L$, where J is the matrix of hopping rates (edge weights). We neglect the self energies; therefore, we will take $D = 0$ and write the Hamiltonian as

$$H = \sum_{nm} (J_{nm} A_{nm} |n\rangle\langle m| + J_{mn} A_{mn} |m\rangle\langle n|). \quad (2)$$

In contrast to CTQW where every J_{nm} is real-valued, CQW allows for complex edge weights, subject to $J_{mn} = J_{nm}^*$, so that the support graph of the walk becomes a directed one (cf. Fig. 1). Specifically, we take

$$H = \begin{bmatrix} 0 & -i & -i & 0 & 0 \\ i & 0 & -i & -i & 0 \\ i & i & 0 & -i & -i \\ 0 & i & i & 0 & -i \\ 0 & 0 & i & i & 0 \end{bmatrix} \quad (3)$$

The choice of the phase $\theta_{nm} = \pi/2$ of complex hopping weights $J_{nm} = |J_{nm}| \exp(i\theta_{nm})$ (with $n > m$) is based upon the general investigations of CQW [41] for a triangular plaquette. It is found that maximum bias in time asymmetry can be obtained at $\theta = \pi/2$ [41]. Remarkably, the spectrum of Hamiltonian with a phase of $\pi/2$ yields has an anti-symmetric structure

$$\lambda_{1,2,3,4,5} = \left(-\sqrt{\frac{1}{2}(7 + \sqrt{37})}, -\sqrt{\frac{1}{2}(7 - \sqrt{37})}, 0, \sqrt{\frac{1}{2}(7 - \sqrt{37})}, \sqrt{\frac{1}{2}(7 + \sqrt{37})} \right). \quad (4)$$

We intuitively assume that a similar choice should yield efficient entanglement transfer along a linear chain of equilateral triangles, too. We numerically examined different choices and verified that our intuition is correct (Some typical results will be given in Sec. III).

H determines the evolution of the initial state $\rho(0)$ by $\rho(t) = U\rho(0)U^\dagger$, where $U := \exp(-iHt)$. Initially, the leftmost pair of sites are entangled in a Bell state, and we aim to transfer the state to the right end of the chain.

Remarkably, CTQW, even with initial coherent superposition states on our linear triangular chain, could not yield pretty good state transfer (PGST) (cf. Fig. 2). The graphs that can support Perfect State Transfer (PST) require to be hermitian, circulant, and to have a non-degenerate spectrum, together with a flat eigenbasis [39]. Alternatively, PST can still be achieved with a non-circulant graph that contains non-zero values on certain off-diagonal elements of its adjacency matrix [40]. From a practical point of view, special graph structures which have PST occupy a large volume with many qubits. Therefore, creating a simpler graph with PGST can be more applicable than using a graph with a PST. Since our proposed adjacency matrix is neither circulant nor has required non-zero off-diagonal elements, we do not expect any PST. Our objective is to explore a chiral linear graph with more compact and practical unidirectional state transfer with high, albeit non-perfect efficiency.

III. RESULTS

We will start with an examination of PTS-breaking in CTQW on the triangular chain as a benchmark of comparison with the results of CQW. We do not need complex edge weights to break PTS in general. The essential mechanism behind PTS breaking is the quantum path interference, for which the required phase difference, or quantum coherence, can be injected into the initial state instead of the edges. Specifically, we consider a qubit which is spatially entangled in two sites in the site basis,

$$|\psi_{\text{spatial}}(0)\rangle = \frac{1}{\sqrt{2}}(|1\rangle - e^{i\phi}|2\rangle) \quad (5)$$

on a regular triangular chain with real-valued hopping weights (we take $J_{nm} = 1$ for simplicity).

We want to transfer the input state to the end-site of the structure. Ideally, we would like to achieve the target state

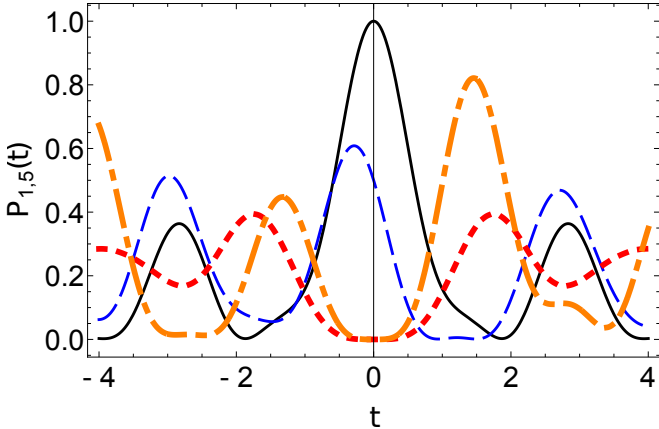


Figure 2. Time dependence of the occupation probabilities $P_{1,5}(t)$ of sites 1 and 5 of a triangular chain with 5 sites, where a particle makes CTQW. For an initially localized particle with initial state $|1\rangle$, $P_1(t)$ and $P_5(t)$ are indicated by black, solid and dotted, red curves, respectively. For a particle initially in a quantum coherent superposition state $|\psi(0)\rangle = (|1\rangle - \exp(i\phi)|2\rangle)/\sqrt{2}$ with $\phi = 3\pi/4$, $P_1(t)$ and $P_5(t)$ are plotted by dashed, blue and dot-dashed, orange curves, respectively.

$|\psi_{\text{target}}\rangle = (|4\rangle - \exp(i\phi)|5\rangle)/\sqrt{2}$. To characterize the performance of the actual process, in addition to the fidelity of state transfer $|\langle\psi_{\text{target}}|\psi(t)\rangle|^2$, we quantify the entanglement transferred to the end of the chain (sites 4 and 5). As we have only a single excitation, the initial state in Eq. (5) evolves into a state in the form

$$|\psi(t)\rangle = (A_1|100\rangle_{123} + A_2|010\rangle_{123} + A_3|001\rangle_{123})|00\rangle_{45} + |000\rangle_{123}(A_4|10\rangle_{45} + A_5|01\rangle_{45}), \quad (6)$$

where A_i are the time dependent coefficients depending on the eigenvalues of the Hamiltonian of the QW.

Tracing out the states of the sites 1, 2 and 3 in the density matrix $\rho(t) = |\psi(t)\rangle\langle\psi(t)|$, we find the reduced density matrix for the sites 4 and 5 in the form

$$\rho_{4,5} = \begin{bmatrix} 1 - a_{44} - a_{55} & 0 & 0 & 0 \\ 0 & a_{44} & a_{45} & 0 \\ 0 & a_{45}^* & a_{55} & 0 \\ 0 & 0 & 0 & 0 \end{bmatrix}, \quad (7)$$

where $a_{ij} = A_i A_j^*$. The simple structure of this matrix remains the same for any chain length.

We can quantify the pairwise entanglement using concurrence [55]. For a state ρ , concurrence is defined as

$$C(\rho) = \max(0, \lambda_1 - \lambda_2 - \lambda_3 - \lambda_4), \quad (8)$$

where $\tilde{\rho}$ is the spin-flipped state, and $\{\lambda_i\}$ is the set of eigenvalues of $R = (\rho^{1/2}\tilde{\rho}\rho^{1/2})^{1/2}$ arranged in non-increasing order. With this at hand, $C_{i=4,j=5}$ is found to take the form

$$C_{4,5} = 2\text{Max}(0, \sqrt{\rho_{44}\rho_{55}}, |\rho_{45}|). \quad (9)$$

Using the adjacency matrix H in Eq. (3) and the initial state $\rho(0)$ in Eq. (5), with any ϕ , the dynamics of the entanglement between pairs of sites of the system can be calculated numerically for any value of t . In Appendix B, we provide approximate analytical trends for such quantity, obtained by making use of a power-series approach. We will also investigate the transport of the initial entangled Bell site-state from the sites 1 and 2 to sites 4 and 5 in CQW. We will compare the speed and concurrence of the transfer with the benchmark case of CTQW with the initial state in Eq. (5).

A. PTS breaking and entanglement transfer in CTQW on a triangular chain

To appreciate the role of the initial phase in Eq. (5) on the state transfer and PTS breaking in CTQW on the triangular chain, let's start with the initial state $|\psi(0)\rangle = |1\rangle$. The occupation probabilities $P_i = \langle i|\rho(t)|i\rangle$ of the sites $i = 1$ (solid, black) and $i = 5$ (dotted, red) are shown in Fig. 2, where mirror symmetry in the behaviour of the probability distribution with respect to time can be seen. Transfer from the initially occupied site $|1\rangle$ to the rightmost site $|5\rangle$ is found to be weak (less than 45% at any time).

If we use the initial state given in Eq. (5) with the hamiltonian Eq. (2), in addition to be able to control path interference, PTS can be broken depending on the initial phase ϕ . We have numerically compared $P_5(t)$ for different ϕ and found that $\phi = 3\pi/4$ gives the largest occupation of site $|5\rangle$. Fig. 2 shows $P_1(t)$ (dotted, red) and $P_5(t)$ (dot-dashed, orange) for $\phi = 3\pi/4$, where time reversal asymmetry, $P(t) \neq P(-t)$ emerges. Population transfer is significantly enhanced using such a quantum superposition state initially. We conclude that transferring a particle from the left end of the chain to a site at the right end is more successful by injecting the particle simultaneously at two sites with a certain quantum coherence relative to starting a well-localized particle at a single site. Let's now explore if similar advantages can be found in the entanglement transfer.

Fig. 3 shows that the concurrence is optimum for $\phi = \pm 3\pi/4$ with a value $C_{4,5}(1.12) \sim 0.8$. Therefore, for pairwise entanglement transfer, $\phi = 3\pi/4$ gives the most advantageous initial state. Remarkably, the same initial state yields the optimum population transfer (at a different time), too. A natural question to ask is if there is a fundamental connection of the critical phase $\phi = 3\pi/4$ and PTS breaking in CTQW.

We can quantify the bias between the forward and backward time evolutions using the Bures distance between the states $\rho(t)$ and $\rho(-t)$. Bures distance is defined by [56–58]

$$D_B(\rho, \sigma)^2 = 2(1 - \sqrt{F(\rho, \sigma)}), \quad (10)$$

where

$$F(\rho, \sigma) = [\text{Tr}(\sqrt{\sqrt{\rho}\sigma\sqrt{\rho}})]^2 \quad (11)$$

is the fidelity [72].

In Fig. 4 the Bures distance D_B is calculated for different ϕ . For the phases 0 and $\pm\pi$ the PTS is not broken and the Bures

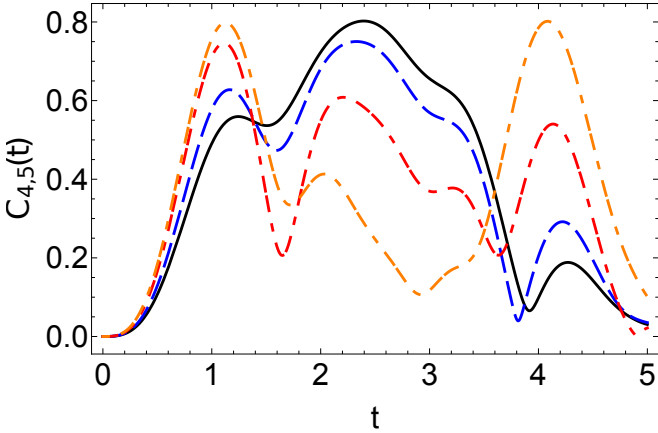


Figure 3. Time dependence of the concurrence $C_{4,5}(t)$ of the state of sites $|4\rangle$ and $|5\rangle$ for an initially entangled state of the sites $|1\rangle$ and $|2\rangle$ of a particle that makes CTQW on a triangular chain of $N = 5$ sites. Different curves stand for the initial states $|\psi(0)\rangle = (|1\rangle - \exp(i\phi)|2\rangle)/\sqrt{2}$ with $\phi = \pi/4$ (solid, black), $\phi = \pm\pi/3$ (dashed, blue), $\phi = \pm\pi/2$ (dot-dashed, red), $\phi = \pm 3\pi/4$ (dotted, orange).

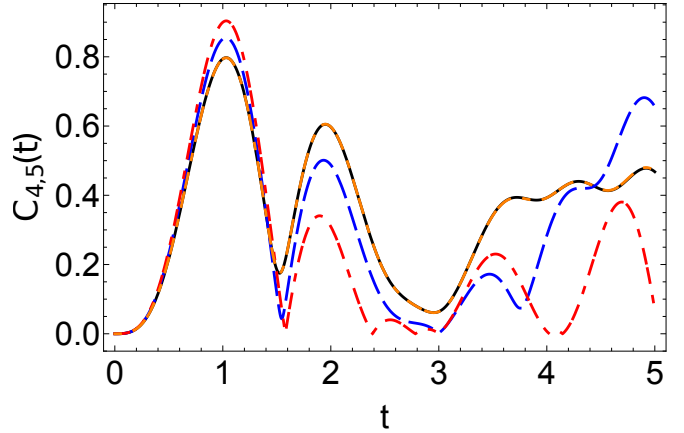


Figure 5. Time dependence of the concurrence $C_{4,5}$ measuring the pairwise entanglement between the sites $|4\rangle$ and $|5\rangle$ of a triangular chain of $N = 5$ sites over which an initial maximally entangled Bell state $(|1\rangle + |2\rangle)/\sqrt{2}$ of the sites 1 and 2 undergoes CQW. Different curves are for the different complex hopping coefficients of the CQW with the phases $\theta = \pi/4$ (solid, black), $\theta = \pm\pi/3$ (dashed, blue), $\theta = \pm\pi/2$ (dot-dashed, red), $\theta = \pm 3\pi/4$ (dot-dashed orange on coloured version); same as $\theta = \pi/4$.

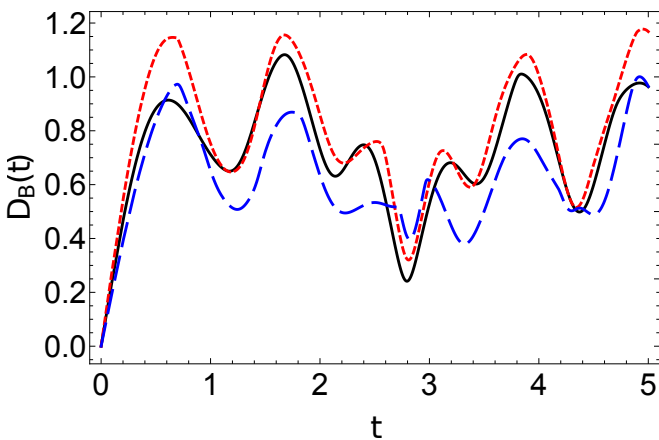


Figure 4. Time dependence of the Bures distance between the forward and backward evolved density matrices $\rho(t)$ and $\rho(-t)$, for a CTQW on a triangular chain. The curves are for the coherence phases ϕ in the initial state $|\psi(0)\rangle = (|1\rangle - \exp(i\phi)|2\rangle)/\sqrt{2}$ with $\phi = \pm\pi/3$ (solid, black), $\phi = \pm\pi/2$ (dotted, red), and $\phi = \pm 3\pi/4$ (dashed blue). The Bures distance for the phases $\phi = 0$ and $\phi = \pm\pi$ are zero.

distance is zero. The largest bias in forward and backward time evolution is found for $\phi = \pi/2$, which is different than the critical phase $\phi = 3\pi/4$ for optimum population and entanglement transfer in CTQW over a triangular chain. We conclude that, instead of utilizing the broken-PTS, CTQW exploits the path interference for efficient state transfer.

B. PTS breaking and entanglement transfer in CQW on a triangular chain and comparison with CTQW

For CQW, we plot the concurrence in Fig. 5 by using an initial Bell state with $\phi = \pi$ in Eq. (5) and different θ in Eq. (3). We see that the concurrence is largest for $\theta = \pi/2$ with a value $C_{4,5}(1.02) \sim 0.9$, indicating that CQW has a slight time advantage ($\Delta t \sim 0.1$) along with a significantly higher quality transfer of entanglement compared to CTQW (cf. Fig. 3). Without plotting, we state here that similar conclusion is applicable to occupation probabilities, too. We found that CQW with $\theta = \pi/2$ yields near perfect ($P_5 \sim 0.95$) state transfer $|1\rangle \rightarrow |5\rangle$ at $t \sim 1.64$.

We calculated the concurrences for $\phi = \pi/4$, $\phi = \pi/3$, $\phi = \pi/2$, $\phi = 3\pi/4$ and looked for the optimum θ values. We have found that for the state ($\phi = \pi$) initial Bell state, $\theta = \pi/2$ gives the optimum (maximum) concurrence $C_{4,5}(1.02) \sim 0.9$.

We plot the Bures distance $D_B(t)$ in Fig. 6, which shows that $D_B(t)$ is maximum for $\theta = \pm\pi/2$ (dot-dashed, orange). Remarkably, maximum broken PTS in the CTQW is found for $\phi = \pi/2$. This suggests that $\phi = \theta = \pm\pi/2$ is an optimal choice for the broken-PTS condition both for CTQW and CQW over a triangular chain. The critical angle of maximum time-reversal asymmetry however coincides with a critical angle of optimum state transfer only for the CQW.

In Fig. 7, the concurrences for CQW and CTQW with an initial state of $(|1\rangle + |2\rangle)/\sqrt{2}$ are plotted. The solid red curve represents the CQW case and the dashed blue line is for the CTQW case. This plot also demonstrates the broken-PTS in the CQW case. Here, one can notice the relatively higher entanglement transfer quality in CQW. In addition, the transfer time is relatively shorter in the case of CQW by $\Delta t \sim 0.4$.

To demonstrate the uni-directionality of the entanglement transfer, we plot the dynamics of the concurrences $C_{i,j}$ that

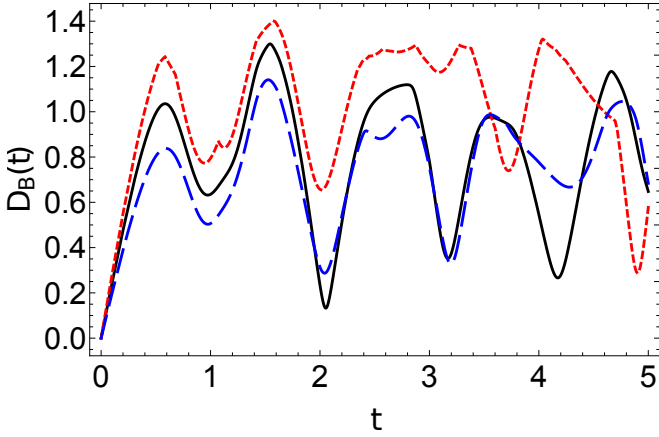


Figure 6. Time dependence of the Bures distance $D_B(t)$ between the forward and backward evolved density matrices $\rho(t)$ and $\rho(-t)$, respectively, for a CQW on a triangular chain of $N = 5$ sites. Initially the quantum walker is in a maximally entangled Bell state $(|1\rangle + |2\rangle)/\sqrt{2}$. Different curves are for chains with different complex hopping coefficients of phases $\theta = \pm\pi/3$ (solid, black), $\theta = \pm\pi/2$ (dotted, red) and $\theta = \pm 3\pi/4$ (dashed, blue). The Bures distance for the phases $\theta = 0$ and $\pm\pi$ are zero; and for $\theta = \pi/4$ $D_B(t)$ is the same as that of $\theta = 3\pi/4$.

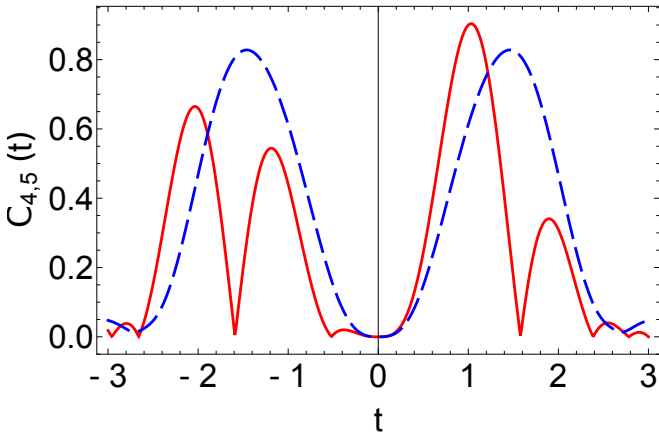


Figure 7. Time(t) dependence of the concurrence $C_{4,5}(t)$ to measure the entanglement between the sites $|4\rangle$ and $|5\rangle$ for an initially maximally entangled Bell state $(|1\rangle + |2\rangle)/\sqrt{2}$ of the sites $|1\rangle$ and $|2\rangle$ of a particle that makes CTQW (dashed, blue) and CQW (solid, red) with $\theta = \pi/2$ on a triangular chain of $N = 5$ sites. We take the phases of the complex hopping coefficients as $\theta = \pi/2$ for CQW; while for CTQW hopping coefficients are real with $\theta = 0$.

measure entanglement between every pair of sites (i, j) of the triangular chain in Fig. 8. One can see that the unidirectional transfer of entanglement from the sites $(|1\rangle, |2\rangle)$ spreads over the system while maintaining a unidirectional movement towards the end of the chain. Although a spread over the system is present, general movement of the peaks of the probability distributions can be interpreted as the dynamics $(|1\rangle, |2\rangle) \rightarrow (|2\rangle, |3\rangle) \rightarrow (|2\rangle, |4\rangle) \rightarrow (|3\rangle, |4\rangle) \rightarrow (|4\rangle, |5\rangle)$.

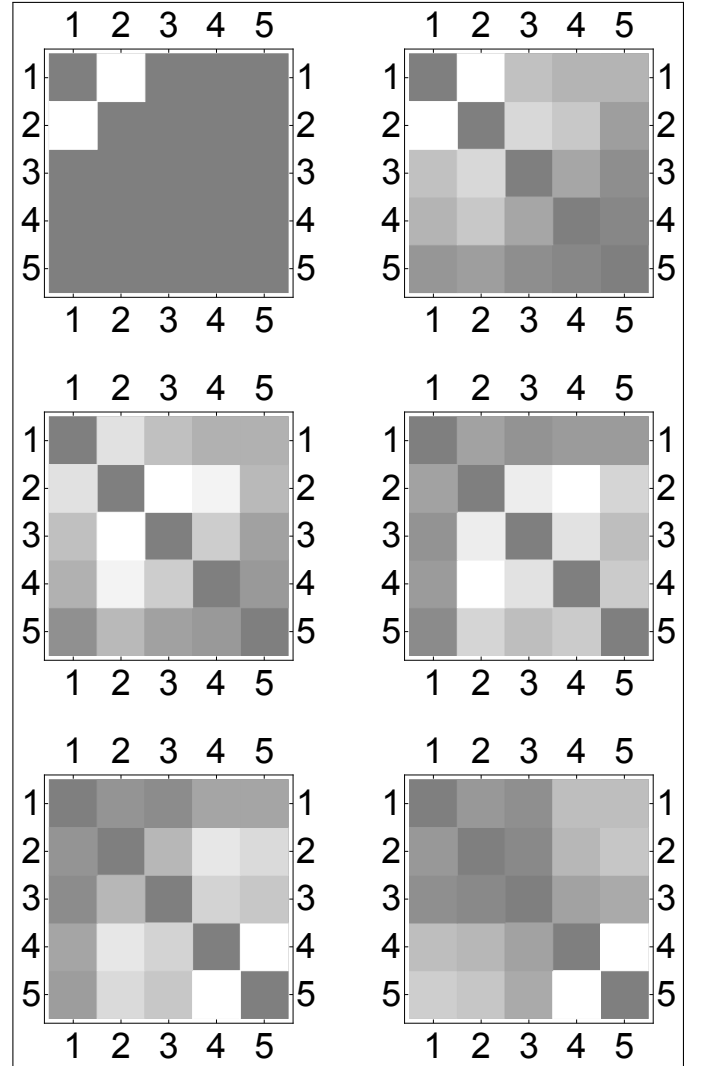


Figure 8. The time evolution of concurrence $C_{i,j}$, measuring the pairwise entanglement between the sites $|i\rangle$ and $|j\rangle$, is shown as a matrix with $i, j = 1..5$. Colors from light to dark scale with 1 to 0, respectively. Initially (at $t = 0$), the quantum walker is injected in the maximally entangled Bell state of the sites 1 and 2 with $C_{1,2} = 1$ (upperleft panel) to undergo CQW with complex hopping coefficients with phase $\theta = \pi/2$. As the time progresses, one can notice the unidirectional transfer of entanglement (light colored pair of squares) to the rightmost sites 4 and 5. The panels are for the $t = 0$ (upper left), $t = 0.2$ (upper right), $t = 0.4$ (middle left), $t = 0.6$ (middle right), $t = 0.8$ (bottom left), and $t = 1$ (bottom right).

C. Transfer of mixed Werner-States on the triangular chain

Having demonstrated the role of pure entangled states under the CQW scheme, it is natural to investigate the behavior of Werner-type mixed states under CQW with $\theta = \pi/2$ phase [73]. We define a Werner state as

$$\rho_{\text{Werner}}(b) = b\rho(0) + (1 - b)\rho_{\text{mixed}}, \quad (12)$$

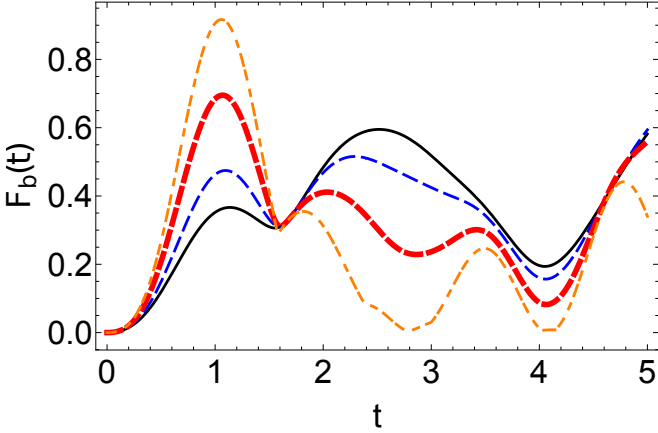


Figure 9. Time dependence of the Fidelity $F(\rho(t), \rho_{\text{target}})$ between $\rho(t)$ and ρ_{Werner} as a function of time t with an initial Werner state under the scheme of CQW on a triangular chain of $N = 5$ sites with complex edge weights of phase $\theta = \pi/2$. Where $b = -1/4$ as solid black, $b = 0$ as dashed blue, $b = 1/2$ as thick dashed red and finally, maximally entangled bell state $b = 1$ is dot-dashed orange.

where ρ_{mixed} is the maximally mixed state

$$\rho_{\text{mixed}} = \frac{1}{2} \sum_{i=1}^2 |i\rangle \langle i|. \quad (13)$$

We use the maximally entangled state $|\psi(0)\rangle = (|0\rangle + |1\rangle)/\sqrt{2}$ to define the initial state density matrix $\rho(0) = |\psi(0)\rangle \langle \psi(0)|$.

To investigate the behaviour of entanglement transfer with respect to time, we calculate the fidelity $F(\rho(t), \rho_{\text{target}})$ as in Eq. (11) with the matrices $\rho(t)$ and ρ_{target} . Here, ρ_{target} represents the desired ideally transferred state

$$\rho_{\text{target}} = \frac{1}{2} \begin{bmatrix} 0 & 0 & 0 & 0 & 0 \\ 0 & 0 & 0 & 0 & 0 \\ 0 & 0 & 0 & 0 & 0 \\ 0 & 0 & 0 & 1 & b \\ 0 & 0 & 0 & b & 1 \end{bmatrix}. \quad (14)$$

In Fig. 9, we plot the time behaviour of the Fidelity, $F(\rho(t), \rho_{\text{target}})$, for different b values. Clearly, the pure maximally entangled state $\rho_{\text{Werner}}(b = 1) = \rho(t = 0)$ yields the best entanglement transfer. On the contrary, no transfer occurs at the maximally mixed state $\rho_{\text{Werner}}(b = 0) = \rho_{\text{mixed}}$.

D. Scaling of entanglement transfer quality and time with respect to the chain size

Until now, state transfer on $N = 5$ chains was discussed. In this section, we calculate the scaling of the transfer time with respect to the chain size. As previously discussed, one can take the last two site states in the site basis and map 2×2 matrix to 4×4 computational basis density matrix $\rho_{\text{comp}}^{N-1, N}(t)$. Here, we calculate the concurrence up to $N = 77$ and find the first maximum. In Fig. 10a, one can appreciate that the transfer time scales linearly with respect to the chain size in accordance

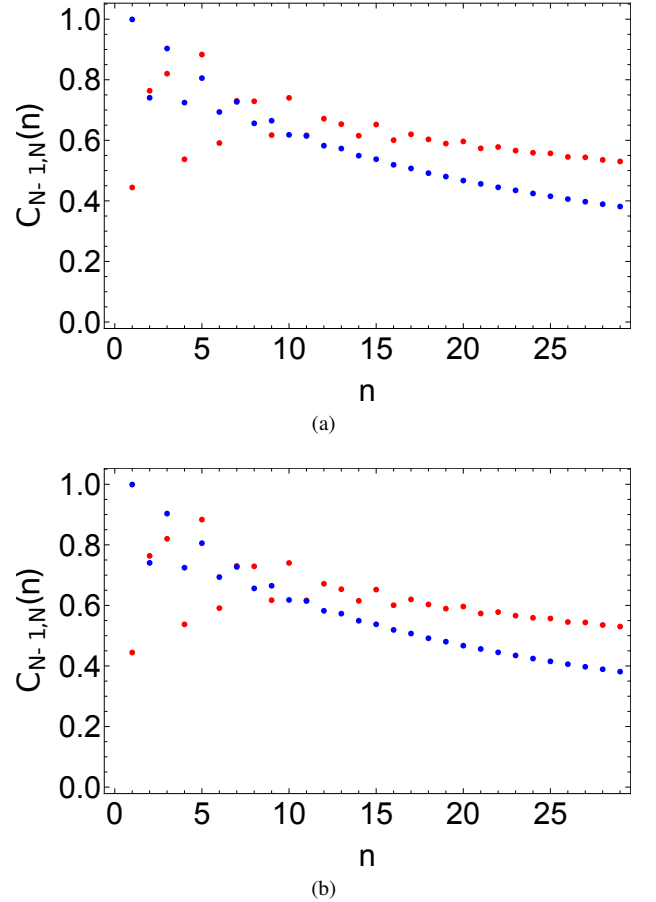
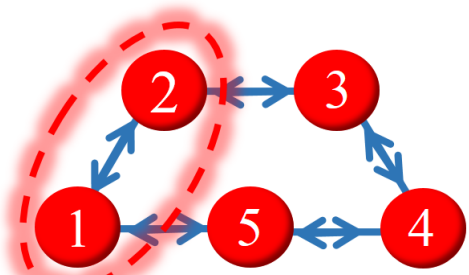


Figure 10. (a) Scaling of state transfer time with respect to the chain size. Red dots represent $\theta = 0$ and blue dots represent $\theta = \pi/2$ (b) Concurrence value at the state transfer time. Red dots represent $\theta = 0$ and blue dots represent $\theta = \pi/2$

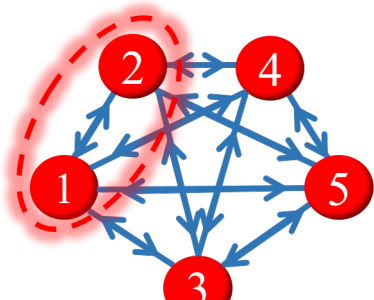
with previous works [74–76]. However, as the chain-size gets larger, one can see an apparent decrease of the entanglement quality along with the poor quality of entanglement for an even number of vertices, as expected from PST-graph conditions in Fig. 10b.

IV. CONCLUSION

We explored the transfer of spatial entanglement of a single particle undergoing CQW on a triangular chain. To appreciate the advantages of CQW, we first considered the case of CTQW. We found that particle transfer to the end of the chain is more successful if the particle is injected simultaneously from the leftmost pair of sites in a specific quantum (Bell-type) superposition state. The success, measured by the rightmost site's occupation probability, depends on the phase ϕ of the initial quantum coherent superposition. For the same ϕ , but at a different time, transfer of the entire state, which is a maximally entangled state, is also the most successful. Using the Bures distance between the forward and backward time evolved states, we examined the dynamics of PTS breaking at different



(a)



(b)

Figure 11. (a) Graph of a linear chain of 5 vertices arranged as an odd number cycle. (b) Graph of a linear chain of 5 vortices arranged as a hexagon with five pointed star-like diagonal connections.

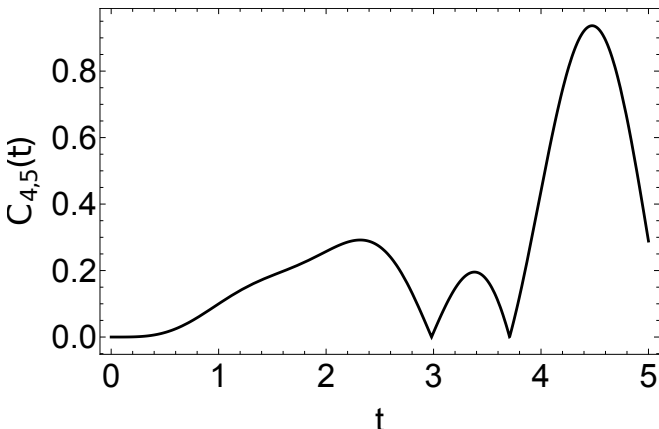


Figure 12. Time(t) dependence of the concurrence $C_{4,5}(t)$ to measure the entanglement between the sites $|4\rangle$ and $|5\rangle$ on a 5×5 circulant graph with only nearest-neighbour interactions for an initially maximally entangled Bell state $(|1\rangle + |2\rangle)/\sqrt{2}$ of the sites $|1\rangle$ and $|2\rangle$ of a particle that makes CTQW.

ϕ . Though CTQW can break the PTS at a certain ϕ , these phases are not critical for an optimal state transfer. The essential mechanism behind the quality of state transfer via CTQW is path interference.

Similar investigations for the CQW revealed that CQW is superior to CTQW in population and entanglement transfers

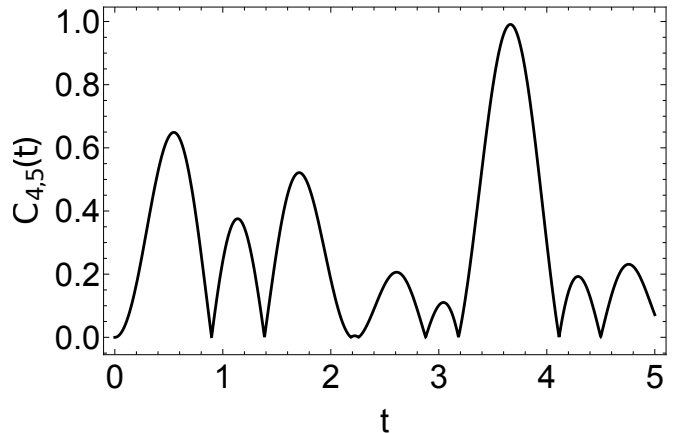


Figure 13. Time(t) dependence of the concurrence $C_{4,5}(t)$ to measure the entanglement between the sites $|4\rangle$ and $|5\rangle$ on a complete hexagonal graph for an initially maximally entangled Bell state $(|1\rangle + |2\rangle)/\sqrt{2}$ of the sites $|1\rangle$ and $|2\rangle$ of a particle that makes CTQW.

efficiency while the speeds are comparable for short chains, confirming the previous results [41, 42]. Calculating the Bures distance, we justified that CQW exploits broken PTS to further enhance the state transfer quality. Remarkably, using the phase θ of the complex edge weights in CQW, the state transfer's success for different ϕ can be optimized, which is not possible with CTQW. When longer chains were considered, the linear scaling of the state transfer speed results agrees with previous works [74–76]. In addition, we explored the behavior of various mixed Werner States under our chiral quantum walk scheme. We found that the purest maximally entangled state yields the best state transfer.

Our results can be significant fundamentally to illuminate the interplay of PTS breaking and entanglement transfer, and practically to design optimum chiral lattices for long-distance transfer of multipartite entangled states in physical platforms such as plasmonic non-Hermitian coupled waveguides [67], ultracold atomic optical lattices [63], photonic-spin waveguides [62], or quantum superconducting circuits [59, 60].

Since the usage of weakly coupled endpoints in spin chains display PGST behavior [7, 28–31], in further studies, one can investigate the effect of this scheme on entanglement transfer on the triangular chain structure. In addition, it would be interesting to investigate the effect of projective measurements on our scheme in a future work [32].

V. ACKNOWLEDGEMENTS

The authors thank Tony John George Apollaro and Deniz N. Bozkurt for fruitful discussions.

Appendix A PERFECT STATE AND ENTANGLEMENT TRANSFER ON CIRCULANT GRAPHS

We present perfect state and entanglement transfer on some circulant graphs in this appendix. Such graphs occupy a relatively large space than linear triangular chains to transfer a state over the same distance and require more qubits to implement. For example, we take a 5×5 circulant graph shown in Fig.11a with only nearest-neighbor interactions. The adjacency matrix for such a graph is

$$A = \begin{bmatrix} 0 & -i & 0 & 0 & -i \\ i & 0 & -i & 0 & 0 \\ 0 & i & 0 & -i & 0 \\ 0 & 0 & i & 0 & -i \\ i & 0 & 0 & i & 0 \end{bmatrix}. \quad (15)$$

Fig. 12 shows that the entanglement transfer on such a graph is nearly perfect with a concurrence of $C \sim 0.93$ at $t \sim 4.5$.

Another example is a hexagonal graph with diagonal connections which is sketched on Fig.11b. This graph contains three triangular plaquettes, but being circulant comes with the cost of more edges. The adjacency matrix reads

$$A = \begin{bmatrix} 0 & -i & -i & -i & -i \\ i & 0 & -i & -i & -i \\ i & i & 0 & -i & -i \\ i & i & i & 0 & -i \\ i & i & i & i & 0 \end{bmatrix}. \quad (16)$$

Fig. 13 presents the possibility of nearly perfect entanglement transfer with a concurrence of $C_{4,5} \sim 1$ at $t \sim 3.7$.

Appendix B MATRIX EXPONENTIAL EXPANSION FOR CONCURRENCE CALCULATION

When we introduce the initial state in Eq. (5), and evolve the density matrix according to the Hamiltonian in Eq. (3) we get expressions that are too cumbersome to present here. We calculate the concurrence by expanding the time evolution operator up to 7th order in t . As seen in Fig. 14, such approximation closely agrees with the numerical calculations of the concurrence for $t \lesssim 1$. The expressions for arbitrary density matrix elements are too complicated and not illuminating. Analytical approach is still valuable to estimate the time and value of the first peak of the concurrence.

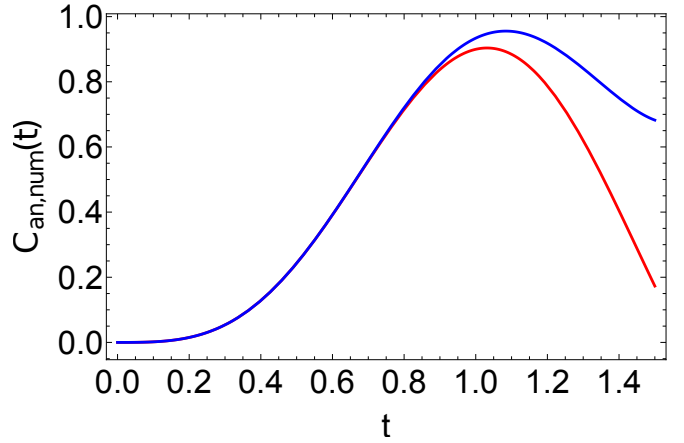


Figure 14. This figure shows the time dependence of the numerically calculated concurrence (solid red curve) and the approximation of the analytic concurrence obtained by expanding the time evolution operator to the 7th power of time. (solid blue curve).

[1] C. H. Bennett and D. P. DiVincenzo, *Nature* **404**, 247 (2000).

[2] D. P. DiVincenzo, *Fortschritte der Phys.* **48**, 771 (2000).

[3] H. J. Kimble, *Nature* **453**, 1023 (2008).

[4] S. Bose, *Phys. Rev. Lett.* **91**, 207901 (2003).

[5] M. Christandl, N. Datta, A. Ekert, and A. J. Landahl, *Phys. Rev. Lett.* **92**, 187902 (2004).

[6] C. Albanese, M. Christandl, N. Datta, and A. Ekert, *Phys. Rev. Lett.* **93**, 230502 (2004).

[7] A. Wójcik, T. Łuczak, P. Kurzyński, A. Grudka, T. Gdala, and M. Bednarska, *Phys. Rev. A* **72**, 034303 (2005).

[8] C. Di Franco, M. Paternostro, and M. S. Kim, *Phys. Rev. Lett.* **101**, 230502 (2008).

[9] M. Mohseni, P. Rebentrost, S. Lloyd, and A. Aspuru-Guzik, *J. Chem. Phys.* **129**, 174106 (2008).

[10] T. J. G. Apollaro, L. Banchi, A. Cuccoli, R. Vaia, and P. Verrucchi, *Phys. Rev. A* **85**, 052319 (2012).

[11] I. Sinayskiy, A. Marais, F. Petruccione, and A. Ekert, *Phys. Rev. Lett.* **108**, 020602 (2012).

[12] K. Korzekwa, P. Machnikowski, and P. Horodecki, *Phys. Rev. A* **89**, 062301 (2014).

[13] M. P. Estarellas, I. D’Amico, and T. P. Spiller, *Phys. Rev. A* **95**, 042335 (2017).

[14] T. Shi, Y. Li, Z. Song, and C.-P. Sun, *Phys. Rev. A* **71**, 032309 (2005).

[15] M. J. Hartmann, M. E. Reuter, and M. B. Plenio, *New J. Phys.* **8**, 94 (2006).

[16] L. Banchi, T. J. G. Apollaro, A. Cuccoli, R. Vaia, and P. Verrucchi, *Phys. Rev. A* **82**, 052321 (2010).

[17] H. J. Shan, C. M. Dai, H. Z. Shen, and X. X. Yi, *Sci. Rep.* **8**, 13565 (2018).

[18] Z. He, C. Yao, and J. Zou, *Phys. Rev. A* **88**, 044304 (2013).

[19] Z.-X. Man, N. B. An, Y.-J. Xia, and J. Kim, *Phys. Lett. A* **378**, 2063 (2014).

[20] A. Zwick, G. A. Álvarez, G. Bensky, and G. Kurizki, *New J. Phys.* **16**, 065021 (2014).

[21] D.-X. Li, D.-X. Li, X.-M. Liao, X.-M. Liao, X.-Q. Shao, and X.-Q. Shao, *Opt. Express* **27**, 35971 (2019).

[22] Y. Matsuzaki, V. M. Bastidas, Y. Takeuchi, W. J. Munro, and S. Saito, *J. Phys. Soc. Japan* **89**, 044003 (2020).

[23] R. Vieira and G. Rigolin, *Phys. Lett. A* **384**, 126536 (2020).

[24] W.-K. Mok, D. Aghamalyan, J.-B. You, T. Haug, W. Zhang, C. E. Png, and L.-C. Kwek, *Phys. Rev. Res.* **2**, 013369 (2020).

[25] G. De Chiara, D. Rossini, S. Montangero, and R. Fazio, *Phys. Rev. A* **72**, 012323 (2005).

[26] S. Ashhab, *Phys. Rev. A* **92**, 062305 (2015).

[27] Z.-X. Man, N. B. An, Y.-J. Xia, and J. Kim, *Physics Letters A* **378**, 2063 (2014).

[28] L. Campos Venuti, S. M. Giampaolo, F. Illuminati, and P. Zanardi, *Phys. Rev. A* **76**, 052328 (2007).

[29] L. Banchi, T. J. G. Apollaro, A. Cuccoli, R. Vaia, and P. Verrucchi, *New Journal of Physics* **13**, 123006 (2011).

[30] G. Gualdi, V. Kostak, I. Marzoli, and P. Tombesi, *Phys. Rev. A* **78**, 022325 (2008).

[31] S. M. Giampaolo and F. Illuminati, *New Journal of Physics* **12**, 025019 (2010).

[32] Z.-X. Man, N. B. An, Y.-J. Xia, and J. Kim, *Annals of Physics* **351**, 739 (2014).

[33] O. Mülken and A. Blumen, *Phys. Rep.* **502**, 37 (2011).

[34] A. Ambainis, *Int. J. Quantum Inf.* **01**, 507 (2003).

[35] X. Zhan, H. Qin, Z.-h. Bian, J. Li, and P. Xue, *Phys. Rev. A* **90**, 012331 (2014).

[36] M. Štefaňák and S. Skoupý, *Phys. Rev. A* **94**, 022301 (2016).

[37] V. M. Kendon and C. Tamon, *J. Comput. Theor. Nanosci.* **8**, 422 (2011).

[38] S. J. Large, M. S. Underwood, and D. L. Feder, *Phys. Rev. A* **91**, 032319 (2015).

[39] S. Cameron, S. Fehrenbach, L. Granger, O. Hennigh, S. Shrestha, and C. Tamon, *Linear Algebra Appl.* **455**, 115 (2014).

[40] E. Connelly, N. Grammel, M. Kraut, L. Serazo, and C. Tamon, *Linear Algebra Appl.* **531**, 516 (2017).

[41] Z. Zimborás, M. Faccin, Z. Kádár, J. D. Whitfield, B. P. Lanyon, and J. Biamonte, *Sci. Rep.* **3** (2013).

[42] D. Lu, J. D. Biamonte, J. Li, H. Li, T. H. Johnson, V. Bergholm, M. Faccin, Z. Zimborás, R. Laflamme, J. Baugh, and S. Lloyd, *Phys. Rev. A* **93**, 042302 (2016).

[43] T. G. Wong, *J. Phys. A Math. Theor.* **48**, 405303 (2015).

[44] Y. Liu and D. L. Zhou, *Phys. Rev. A* **91**, 052318 (2015).

[45] D. Cozzolino, B. D. Lio, D. Bacco, and L. K. Oxenløwe, *Adv. Quantum Technol.* **2**, 1900038 (2019).

[46] X. S. Liu, G. L. Long, D. M. Tong, and L. Feng, *Phys. Rev. A* **65** (2002).

[47] A. Grudka and A. Wójcik, *Phys. Rev. A* **66** (2002).

[48] X. M. Hu, Y. Guo, B. H. Liu, Y. F. Huang, C. F. Li, and G. C. Guo, *Sci. Adv.* **4**, 10.1126/sciadv.aat9304 (2018).

[49] A. KAY, *International Journal of Quantum Information* **08**, 641 (2010).

[50] A. Kay and M. Ericsson, *New Journal of Physics* **7**, 143 (2005).

[51] T. Giordani, L. Innocenti, A. Suprano, E. Polino, M. Paternostro, N. Spagnolo, F. Sciarrino, and A. Ferraro, *New Journal of Physics* **23**, 023012 (2021).

[52] S. K. Goyal and C. M. Chandrashekhar, *Journal of Physics A: Mathematical and Theoretical* **43**, 235303 (2010).

[53] S. Azzini, S. Mazzucchi, V. Moretti, D. Pastorello, and L. Pavese, *Advanced Quantum Technologies* **3**, 2000014 (2020).

[54] W. Dür, G. Vidal, and J. I. Cirac, *Phys. Rev. A* **62**, 062314 (2000).

[55] W. K. Wootters, *Phys. Rev. Lett.* **80**, 2245 (1998).

[56] R. Jozsa, *J. Mod. Opt.* **41**, 2315 (1994).

[57] M. Hübner, *Phys. Lett. A* **163**, 239 (1992).

[58] M. Hübner, *Phys. Lett. A* **179**, 226 (1993).

[59] A. Vepsäläinen and G. S. Paraoanu, *Adv. Quantum Technol.* **3**, 1900121 (2020).

[60] K. K. W. Ma, *Phys. Rev. A* **102** (2020).

[61] T. Manovitz, Y. Shapira, N. Akerman, A. Stern, and R. Ozeri, *PRX Quantum* **1**, 020303 (2020).

[62] T. Ramos, B. Vermersch, P. Hauke, H. Pichler, and P. Zoller, *Phys. Rev. A* **93**, 062104 (2016).

[63] J. K. Pachos and M. B. Plenio, *Phys. Rev. Lett.* **93**, 056402 (2004).

[64] I. Bloch, J. Dalibard, and W. Zwerger, *Rev. Mod. Phys.* **80**, 885 (2008).

[65] M. Aidelsburger, S. Nascimbene, and N. Goldman, *CR PHYS* **19**, 394 (2018).

[66] E. K. Levi, P. G. Kirton, and B. W. Lovett, *Physical Review A* **94**, 10.1103/physreva.94.032302 (2016).

[67] Z. Fu, N. Fu, H. Zhang, Z. Wang, D. Zhao, and S. Ke, *Appl. Sci.* **10**, 3425 (2020).

[68] J. Kempe, *Contemp. Phys.* **44**, 307 (2003).

[69] A. Sett, H. Pan, P. E. Falloon, and J. B. Wang, *Quantum Inf. Process.* **18** (2019).

[70] E. Farhi and S. Gutmann, *Phys. Rev. A* **58**, 915 (1998).

- [71] A. M. Childs, E. Farhi, and S. Gutmann, *Quantum Inf. Process.* **1**, 35 (2002).
- [72] I. L. C. Michael A. Nielsen, *Quantum Computation and Quantum Information* (Cambridge University Press, Cambridge, 2010).
- [73] R. F. Werner, *Physical Review A* **40**, 4277–4281 (1989).
- [74] S. Lorenzo, T. J. G. Apollaro, S. Paganelli, G. M. Palma, and F. Plastina, *Phys. Rev. A* **91**, 042321 (2015).
- [75] W. J. Chetcuti, C. Sanavio, S. Lorenzo, and T. J. G. Apollaro, *New Journal of Physics* **22**, 033030 (2020).
- [76] S. Lorenzo, T. J. G. Apollaro, A. Trombettoni, and S. Paganelli, *International Journal of Quantum Information* **15**, 1750037 (2017).